ACS APPLIED MATERIALS & INTERFACES
Research Article
www.acsami.org

Metal-Free Doping Process to Enhance the Conductivity of Zinc Oxide Nanorods Retaining the Transparency

Shrabani Panigrahi, Sanjit Sarkar, and Durga Basak*

Department of Solid State Physics, Indian Association for the Cultivation of Science, Jadavpur, Kolkata 700032, India

ABSTRACT: The well-ordered metal oxide nanostructures can be synthesized successfully, but the conductance of these structures is limited, which is a disadvantage for applying these in photovoltaic and display devices. Conductivity of a semiconductor can be improved by using metal doping, but the issue becomes a major challenge in nanostructures since their high surface energy usually hinders any metal doping process. Here we show an entirely new metal-free doping strategy to enhance the current conduction of ZnO nanorods' (NRs) arrays through a sulphidation technique. The process is based on the electronegativity difference between S and O because of which one can expect a rigorous bond rearrangement at the interface and a ZnOS-ZnS composite is formed as O is being partially replaced by S. The current conduction by the metal oxide NRs arrays is significantly enhanced by nearly 4 orders of magnitude without sacrificing the transparency of the NRs arrays. The increased current conduction is assigned due to an increase in the Zn_i concentration as evidenced from the electron paramagnetic resonance measurements. The composite layer grown on p-Si forms a photodiode which is highly sensitive to visible light with a very fast response time.

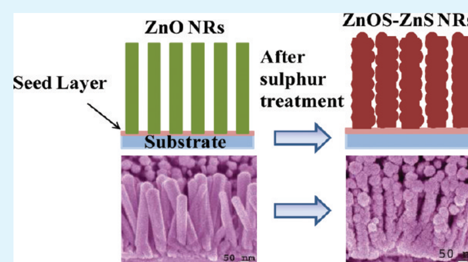

KEYWORDS: *transparent conducting oxide, sulphidation, ZnO nanorods, Zn_i, photodiode*

INTRODUCTION

A major challenge in the field of nanoscaled technology is to tune the device performance by developing nanomaterials that can combine the advantages of both their fascinating properties and device suitability. One-dimensional (1-D) semiconductor materials have thus attracted a great deal of attention because of their potential applications as building blocks for nanoscale devices that are usually not able to be fabricated using bulk or 3-D materials due to their laterally quantum confined electrons. ZnO is probably one among the most popular ingredients which is familiar as one of the most important photonic materials for its numerous application in nanoelectronic devices,[1−8] including optoelectronic applications[9−16] because of its wide band gap (E_g = 3.37 eV at room temperature) and large exciton binding energy (60 meV). However, conductivity of ZnO nanorods (NRs) arrays is still a major technical issue, which is one of the hindrances of ZnO nanostructured -based photovoltaic cells. Usually cationic substitution by a trivalent metal is the doping process which is adopted for ZnO to make it highly conducting.[17] Though there are plenty of reports on highly conducting n-type doped bulk as well as films of ZnO, there are very few reports on doped 1-D ZnO nanostructures.[18−20] Xu et al.[18] have reported that the resistivity can be decreased by almost 100 times by Ga-doping in ZnO nanofibers. The electrical conductivity has been increased by only 30 times by Ni-doping in ZnO nanowires (NWs).[19] Al doping in ZnO NWs has caused 3 orders of increase in the conductivity as reported by Hsu et al.[20] In general, it becomes quite a difficult task to heavily dope 1-D nano-structures, especially because of their higher surface energy as compared to their bulk counterparts, which usually hinders any extrinsic doping process. Therefore, one must think of an intuitive approach of bringing a change in the conductivity utilizing the fascinating properties of ZnO nanostructures. For example, one promising approach is to change the interfacial environment. By surface capping, indeed the properties of ZnO NRs have been found to be improved significantly.[21−26] Different phenomena are known to occur at the interface, such as change in the surface bonding, charge transfer, etc.[25,27] There have been efforts to change the conductivity by manipulating the native defects.[28,29] Here, we report an entirely different strategy of metal-free doping to achieve an enhanced conductivity in ZnO NRs. There are studies where changes in the structural, optical, and electrical properties of ZnO have been reported by S doping.[30−37] Keeping in mind the electronegativity difference between S and O, we expect an intimate mixing at the interface of ZnO and ZnS due to bond rearrangement, which should result in a change in the conductivity. Therefore, we have done a sulphidation treatment of pristine ZnO NRs forming a composite ZnOS-ZnS NRs arrays and have observed that the current conduction by the arrays is significantly enhanced by about 4 orders of magnitude without sacrificing the transparency of the layer. An increase in the Zn_i concentration (which is known to behave as a shallow donor[38]) has been evidenced from the electron paramagnetic resonance (EPR)

Received: February 27, 2012
Accepted: May 2, 2012
Published: May 2, 2012

 © 2012 American Chemical Society

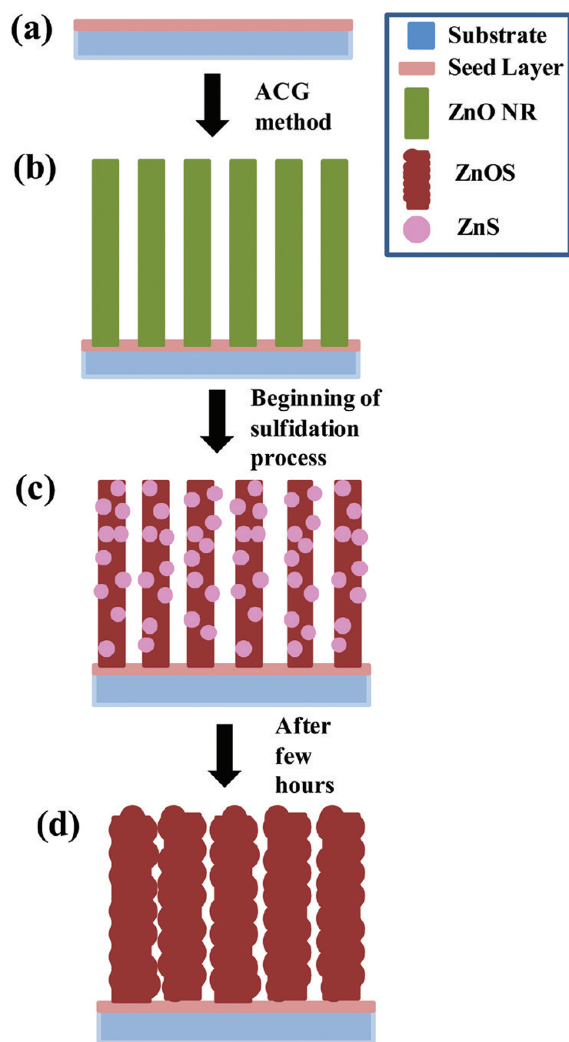

Figure 1. Schematics for the summary of processes used to fabricate transparent, conductive composite NRs arrays.

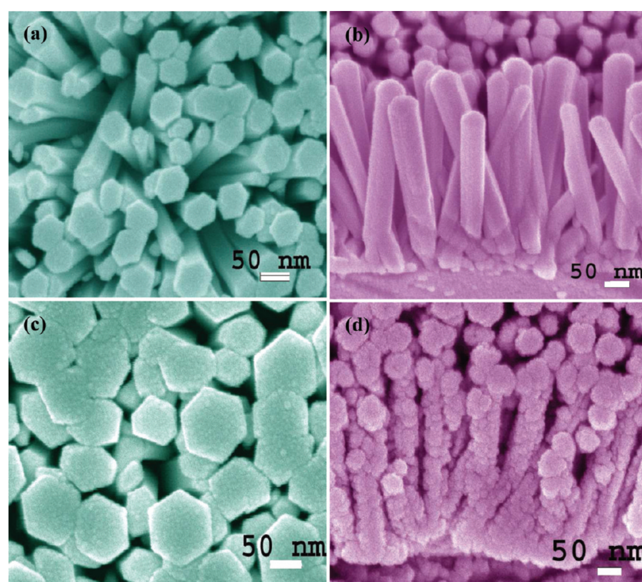

Figure 2. (a) Top view of FESEM of the quasi-vertical ACG-grown pristine ZnO NRs arrays. (b) Cross-sectional FESEM image of the NRs arrays. (c) Top view of FESEM image of a representative composite NRs arrays. (d) Cross-sectional view of a representative composite NRs arrays.

measurements which is responsible for the increased current conduction of the NRs. The composite ZnOS-ZnS NRs arrays when grown on p-Si forms a photodiode which is found to be highly sensitive to the visible light with a very fast response time.

EXPERIMENTAL SECTION

Sulphidation of ZnO NRs was carried out by a two step chemical method. At first, the quasi-vertical ZnO NRs were grown on the glass substrates and as-well-as p-Si substrates by an aqueous chemical growth (ACG) process, as described elsewhere.[39] In brief, first a ZnO seed layer was grown on both of these substrates by thermal decomposition of zinc acetate at 350 °C. Then, the substrates with a seed layer were dipped into an equimolar (20 mM) aqueous solution of zinc acetate [$Zn(CH_3COO)_2{\cdot}2H_2O$] and hexamethylenetetramine [$(CH_2)_6N_4$] at 90 °C for 1 h followed by a rinsing and drying process. For sulphidation, these NRs were dipped into 100 mL of 10 mM aqueous solution of thioacetamide (TAA) (Sigma Aldrich) at 70 °C for 2.5 h, 3.5 h, 5 h, 7 h, and 10 h. Finally, the substrates were removed from the solution, rinsed thoroughly in deionized water, and dried.

The morphologies and microstructures were analyzed by field-emission scanning electron microscopy (FESEM; JEOL model JSM-6700F) and high-resolution transmission electron microscopy [HRTEM, model JEOL JSM-2010], respectively. The structural characterizations of the pristine ZnO and its composite NRs were carried out by X-ray diffractometry (XRD) (model Seifert XDAL 3000). X-ray photoelectron spectroscopy (XPS) (Omicron) was done using an Al−Kα radiation source under 15 kV voltage and 5 mA current conditions. For optical excitation of the sample, a He−Cd laser (Kimmon Koha Co. Ltd.; model KR 1801C) with a wavelength of 325 nm was used. A high-resolution spectrometer (Horiba Jobin Yvon, model iHR 320) together with a photomultiplier tube was used to detect the PL emissions from the samples. The transmission spectra were recorded in the wavelength range 300−800 nm using a UV−vis-NIR spectrophotometer (Perkin Elmer, model Lambda 35). The EPR measurements were performed with a 9.44 GHz spectrometer (JEOL; model JES- FA200) operated at the X-band frequency. For $I-V$ measurements, the dc currents were measured under a certain bias voltage using a Keithley source meter (model 2410). For visible light illumination, a xenon light source (model no. 66902; Newport Corp.) was used with a filter to absorb the UV light below 400 nm. All the measurements were performed at room temperature.

RESULTS AND DISCUSSION

The formation of composite NRs involves two steps as shown schematically in Figure 1. Field emission scanning electron microscopy imaging of the top surface (Figure 2a) and cross section (Figure 2b) of the pristine ZnO NRs arrays show that the diameter of the NRs are in the range of 40−80 nm with a very smooth side wall (Figure 2b). While the top (Figure 2c) and cross-section view (Figure 2d) of the S-treated NRs (hence forth named as composite NRs) show a change in the surface morphology as the diameter of the composite NRs becomes ~90−100 nm for 2.5 h sulphidation. The cross-section view clearly shows that the side walls of the composite NRs become rougher after sulphidation. The microstructure imaging and the crystallinity of the NRs were further confirmed by TEM analyses in Fig. 3a−f. Figure 3a shows the TEM image of a pristine ZnO NR with a diameter of ~80 nm. A high-resolution transmission electron HRTEM image in Figure 3b shows a lattice spacing of 0.26 nm in conformity with the spacing of the

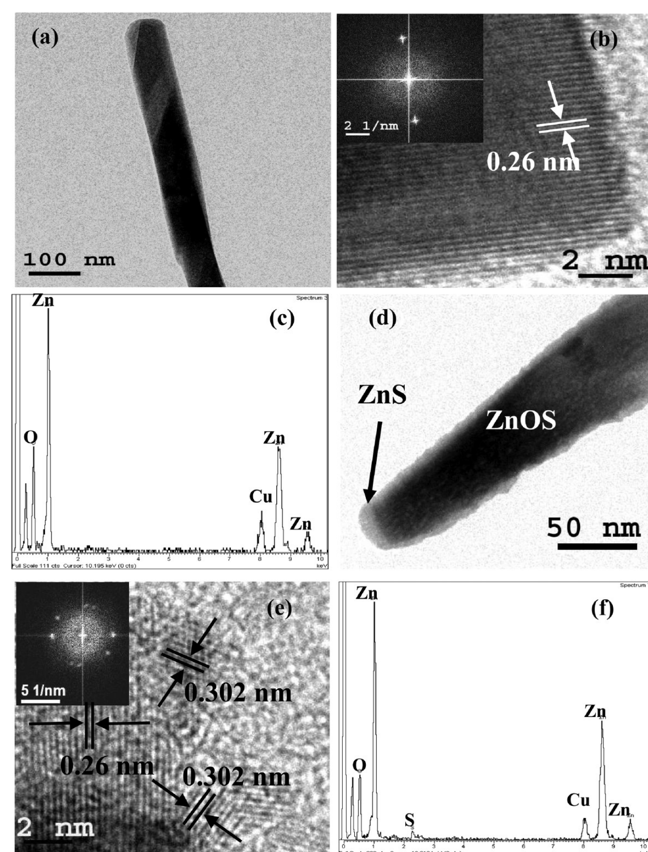

Figure 3. (a) Low-magnification TEM image of a pristine ZnO NR. (b) HRTEM image of the pristine NR showing only one type of lattice fringes of ZnO. Inset: The corresponding FFT pattern showing bright spots corresponding to the hexagonal wurtzite structure of ZnO. (c) The typical EDS result showing the presence of Zn and O elements. (d) TEM micrographs of a representative composite NR. (e) HRTEM image of representative composite NRs showing the lattice fringes corresponding to both ZnS and ZnOS. Inset: The corresponding FFT pattern showing bright and weak spots corresponding to the hexagonal wurtzite structure of ZnO and cubic structure of ZnS, respectively. (f) The corresponding EDS result showing the presence of Zn, S, and O elements.

{0002} plane of wurtzite ZnO structure. The inset in the figure shows the fast Fourier transform (FFT) pattern, which also verifies that the spots are due to a hexagonal wurtzite structure. The EDS spectrum in Figure 3c shows the presence of Zn and O in the pristine sample. Similarly, the TEM and HRTEM images of the composite NRs are shown in parts d and e of Figure 3, respectively. The presence of two different lattice fringes corresponding to the {0002} plane of ZnO and the {111} plane of cubic ZnS confirms the formation of the nanocomposite (Figure 3e). The corresponding FFT pattern clearly shows two sets of diffracted spots in the inset in Figure 3e in which the bright spots correspond to ZnOS and weaker spots to ZnS. The atomic composition of the composite (Figure 3f) shows clear evidences of the presence of Zn, S, and O elements. The structural analyses of the composite NRs are shown in Figure 4. The structure of the pristine and composite NRs can be assigned to the hexagonal wurtzite structure of ZnO. For the composites (shown in Figure 4b–f), an additional peak at $2\theta = 29.4°$ corresponds to the (111) plane of cubic ZnS. The stronger (002) diffraction peak of the

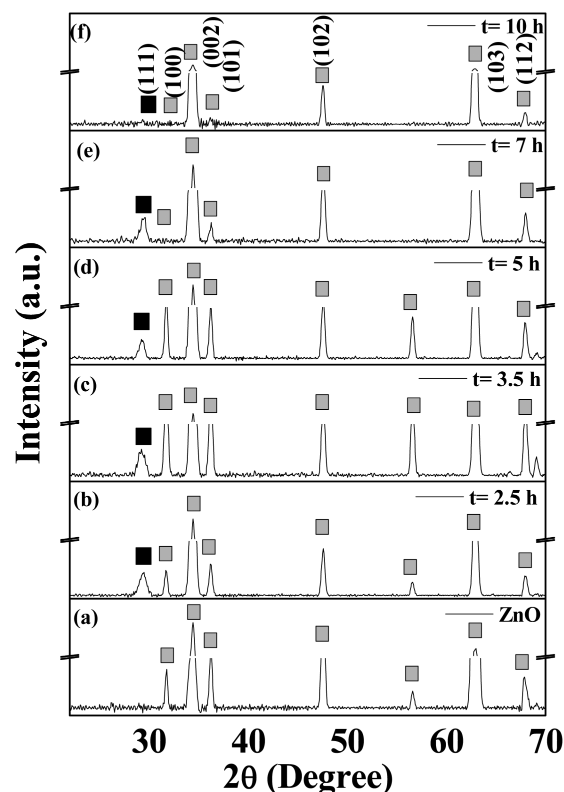

Figure 4. X-ray diffraction patterns of pristine and compsite ZnO NRs. The intensity scale (y-axis) is broken in order to show ZnS peaks. The black box stands for ZnS, and the gray box stands for ZnO/ZnOS peak signal.

Table 1. Dipping Time in TAA, Percentage of ZnOS, and Value of *a* and *c* Parameter of Pristine and Composite ZnO NRs

dipping time in TAA (hrs)	percentage of ZnOS (%)	value of *a* parameter	value of *c* parameter
0	0	3.257	5.186
2.5	96.8	3.252	5.192
3.5	97.3	3.250	5.193
5	97.8	3.250	5.195
7	98.4	3.247	5.199
10	99	3.243	5.206

ZnO NRs indicates a preferential vertical growth direction. The lattice parameters in Table 1 show that the c-axis length gradually increases from 5.186 Å for the pristine ZnO NRs to 5.2056 Å for the 10 h dipped sample. An increase in the lattice parameter indicates the fact that S is substituted in O sites forming ZnOS since the ionic radius of S^{2-} (170 pm) is more than that of O^{2-} (126 pm). This result is in conformity with the results of Pan et al.[40] who also have observed an increased c-axis length with increasing S content in $ZnO_{1-x}S_x$ alloy films fabricated by radio-frequency magnetron sputtering. As the sulphidation process goes on, an increase in the ZnOS content in the composite occurs (Table 1). However, for the 10 h dipped sample, existence of mainly one phase, i.e., ZnOS has been observed which might be highly disordered. Using XPS, the states of atoms on the surface of the NRs arrays were analyzed and the S

dx.doi.org/10.1021/am300348g | ACS Appl. Mater. Interfaces 2012, 4, 2709–2716

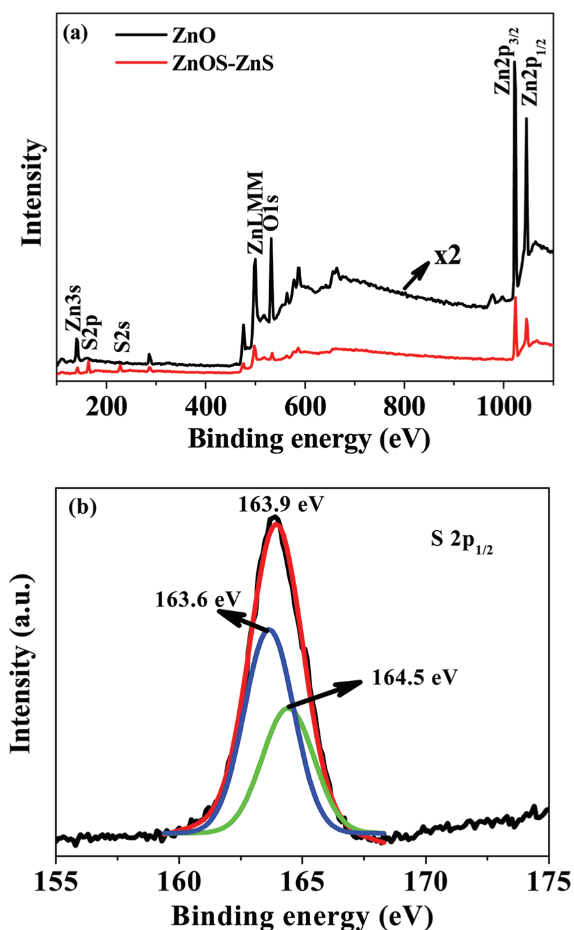

Figure 5. (a) XPS spectra of ZnO and ZnOS-ZnS NRs arrays. (b) Gaussian peak fitting of S $2p_{1/2}$.

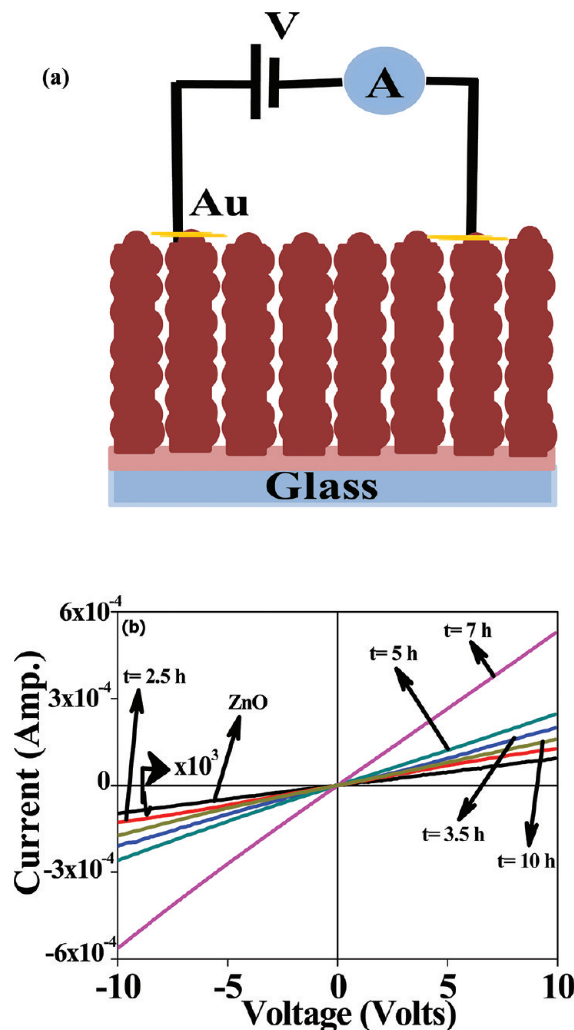

Figure 6. (a) Schematic of the layout of the circuit diagram for $I-V$ measurements. (b) Plots of $I-V$ curves of pristine and composite ZnO NRs arrays in room light.

substitution is further confirmed from the XPS results. Figure 5a shows the spectra of the pristine ZnO and ZnOS-ZnS NRs arrays. In the case of pristine NRs, the peaks located at 1046, 1022, and 532 eV corresponds to the to Zn $2p_{1/2}$, Zn $2p_{3/2}$, and O 1s, respectively. The spectra for the composite show two other peaks at 163.9 and 228.2 eV corresponding to the electronic states of S $2p_{1/2}$ and S 2s, respectively. The S $2p_{1/2}$ peak can further be deconvoluted into two peaks, one at 163.6 eV corresponding to the Zn−S binding energy[41,42] and another at the higher energy side at 164.5 eV corresponding to the O−Zn−S binding energy (shown in Figure 5b).[43] This indicates S remains in two different environments in the composite NRs. Therefore, the sulphidation process takes place in two steps to form ZnOS-ZnS composite:

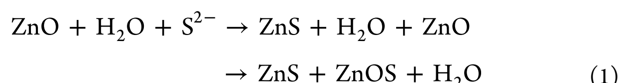

$$ZnO + H_2O + S^{2-} \rightarrow ZnS + H_2O + ZnO \rightarrow ZnS + ZnOS + H_2O \quad (1)$$

Figure 6a shows the setup for the current−voltage ($I-V$) measurements. The $I-V$ characteristics of the pristine and composite NRs arrays in Figure 6b show that the current increases linearly with an increase in the voltage both in forward and reverse bias conditions. The results clearly illustrate that the highest current has been obtained for the 7 h sulphidized sample, which is about 4 orders of magnitude higher compared to that of the pristine NRs. Since conductivity is directly proportional to the current provided the length, area, and bias voltages are constant, it can be said that conductivity of the S treated ZnO NRs arrays is enhanced by 4 orders of magnitude. Our value is much higher than those reported for Ga, Ni, and Al doping as discussed earlier.[18,19] Such huge enhancement is probably due to an increase in the donor concentration in the NRs. A reduction in the electron trap states (i.e., physisorbed O molecules on the surface[39]) as a cause might be ruled out for such an high enhancement in the conductivity. When ZnO is dipped in thioacetamide (CH_3CSNH_2) solution, the S^{2-} ions react with ZnO to form ZnS and subsequently replace O^{2-} to form ZnOS alloy on the surface. Because of the electronegativity difference, excess Zn_i donors might have formed during bond rearrangement. Also in the presence of excess O reducing atmosphere such as NH_3, a lot of Zn_i may be formed.[44] Since Zn_i is known to act as shallow donors in ZnO ,[38] the composite NRs arrays becomes highly conducting. Further insight into the conduction mechanism can be obtained from the EPR spectra shown in Figure 7a. EPR is a measurement technique which gives direct evidence of an ionized defect and thus is used as a strong tool to indentify the defect nature. The EPR spectrum shows a small signal at g (gyromagnetic ratio) ∼ 1.95 for pristine NRs due to the

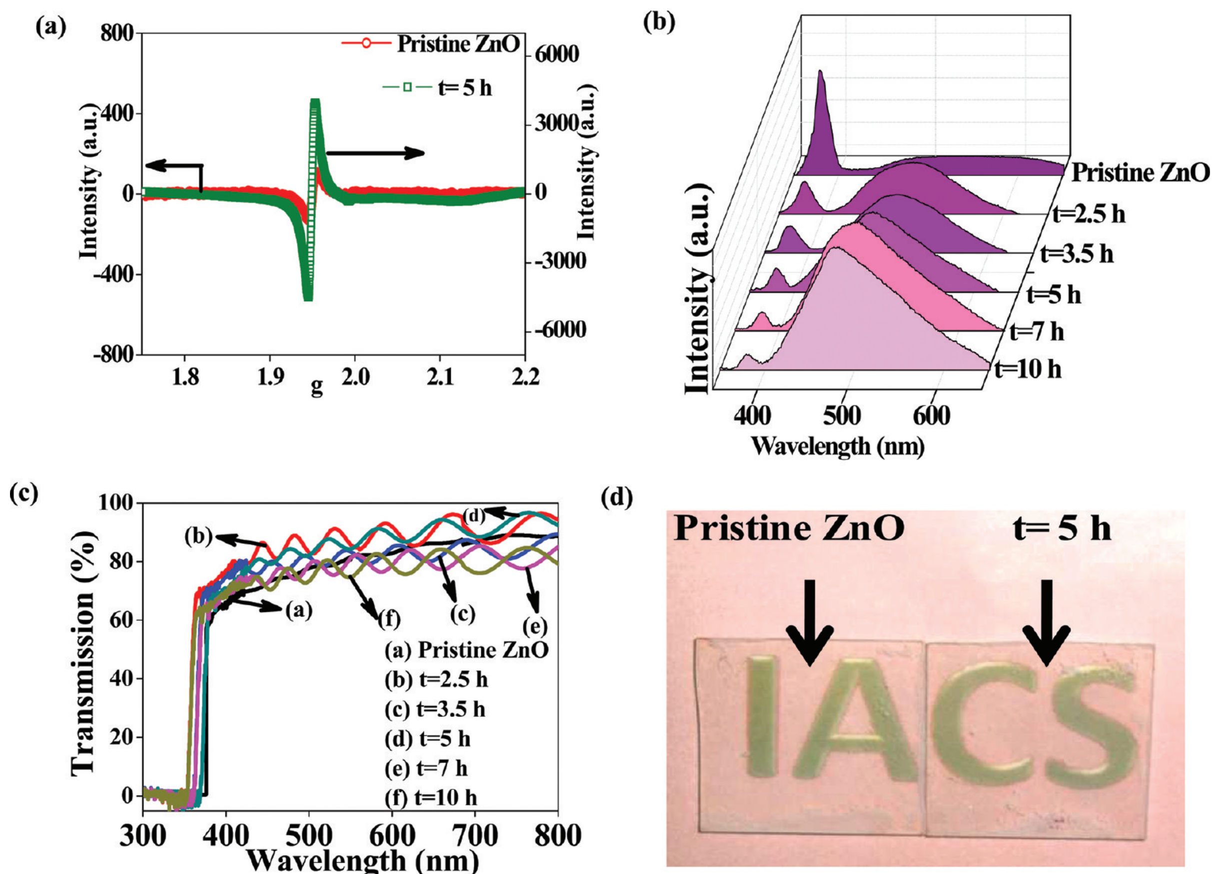

Figure 7. (a) EPR measurement as a function of *g* measured at room temperature. (b) The PL spectra of pristine and composite NRs arrays. (c) Optical transmission spectra of pristine and composite NRs arrays. (d) The digital image showing the transparency of pristine and composite NRs arrays for the name "IACS".

Zn_i type of defects.[45,46] The huge increase in the intensity of the EPR signal of the composite NRs indicates a lot more Zn_i donor defects which are generated probably at the interface due to S treatment. Therefore, our proposition is that the current enhancement is caused by the Zn_i is now supported by the EPR results. The increase in the defects is further demonstrated from the PL results (Fig. 7b). The figure shows that pristine ZnO NRs show a strong, narrow near-band edge (NBE) emission due to the recombination of the free excitons of ZnO[47] and a broad visible emission band due to the oxygen vacancy as well as excess oxygen present in ZnO.[48,49] However, when S is incorporated into ZnO, the NBE emission intensity decreases while the visible defect emission intensity increases with increasing the sulfidation time.[33] The difference in the PL spectrum between the pristine and composite sample can be explained as follows. Incorporation of S atoms into ZnO causes formation of new in-gap energy levels causing radiative recombinations, which changes the intensity of the UV as well as visible emission.[33]

These highly conducting NRs' arrays are nearly 80% transparent in the visible region (400−800 nm) as evidenced from the transparency curves in Figure 7c. At first, the transparency slightly increases for samples with lower dipping time and then slightly decreases with increasing the dipping time. A similar change in the transparency has been observed in the case of Al and Sb doped ZnO NRs,[20,50] while in the case of Nb doped ZnO films transparency remains very high.[51] The digital image in Figure 7d simultaneously verifies that the transparency is comparable as the acronym "IACS" appears to be equally prominent through the films consisting of pristine and composite NRs arrays.

The dark and photo (visible light 400−800 nm) *I*−*V* curves for the diodes in Figure 8a−d clearly show that under a forward bias condition, no significant change in the current takes place under visible light illumination, while the current increases drastically as the reverse bias increases.[52,53] Our results show that the ratio I_{ph}/I_d at −10 V for almost all the junctions is much more than that of the forward bias conditions. The reverse leakage current under dark condition is found to be larger for 7 and 10 h dipped samples. Therefore, *I*−*V* results show that the diodes are highly visible light sensitive. In order to explain the reason, we have performed photocurrent measurements. The photocurrent spectra of the composite samples were measured by illuminating the samples for 1 min with lights of different wavelengths from 300 to 800 nm for a bias voltage of 5 V. Figure 8e (representative curves for 5 and 7 h dipped samples) shows that there is a broad peak in the visible region from 400 to 800 nm, i.e., below the band gap of ZnO or ZnS. The current in this region is caused by the photocarriers released from the in-gap defect states. This indicates that the carriers can be generated in the composite NRs under the visible light illumination. The schematic energy band alignment of ZnOS-ZnS NRs and p-Si is shown

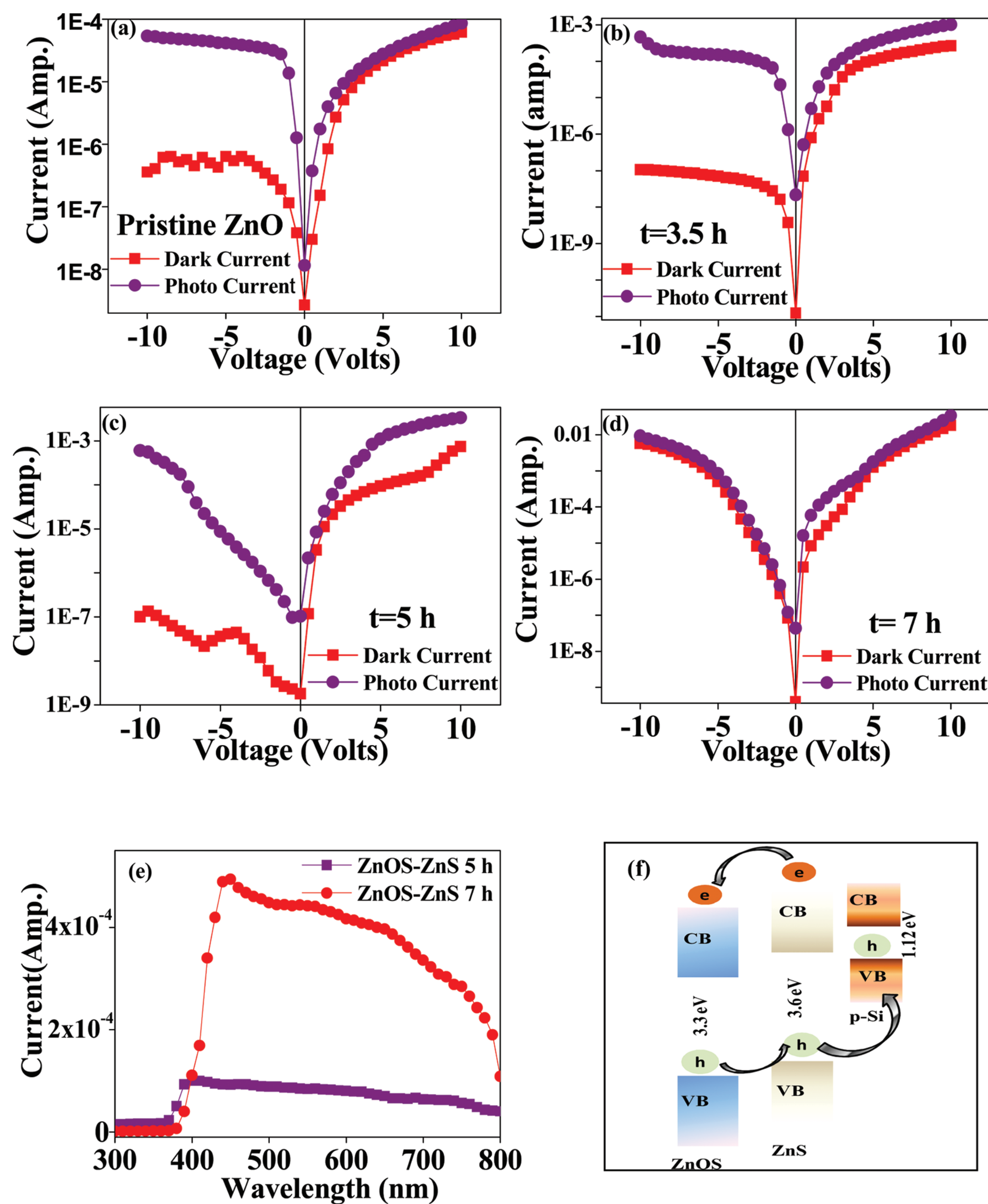

Figure 8. (a−d) Semi log plots of $I-V$ characteristics measured in the dark and under illumination (visible light) for pristine and composite NRs. (e) The photocurrent spectra of 5 and 7 h dipped samples. (f) Schematic energy band diagram of n-ZnOS-ZnS/p-Si heterojunction.

in Figure 8f. The band alignment is such that the electrons-holes are easily separated under biased conditions. Under illumination, the photogenerated electrons are drifted towards the positive electrode and consequently the photocurrent increases with increasing reverse bias because of the electric field strength inside the depletion region increases with applied voltage.[52]

The photo current transient measurements of the n-ZnOS-ZnS NRs/p-Si heterojunction in Figure 9a show that the heterojunction can reversibly be turned "on" and "off" for a duration of 20 s each under visible light illumination (400−800 nm) with a bias voltage of −5 V. It can also be seen that the photoresponse of the NRs are highly stable and reproducible. The possible reasons for the current fluctuation are surface species absorption/desorption or appearance of defects.[54] From the enlarged view of the single "on"-"off" cycle (Figure 9b), the time for rise (t_r) and decay (t_d) of the current are seen to be shorter than 0.1 s. The fast visible photoresponse of the conducting composite NRs indicate that these photodiodes can be used as optical switches as well. These composite NRs-based photodiode shows an improved responsivity compared to previously reported devices such as ZnO NWs-based UV sensors,[55] In_2Se_3 NWs-based visible light photodetector,[56] or in the case of white light photoconductor using CdS nanobelt.[57] The charge transfer at the interface is also supported by the report of photocatalytic activity due to S-doping in TiO_2 nanoparticle indicating enhanced electron transfer from TiO_2.[58]

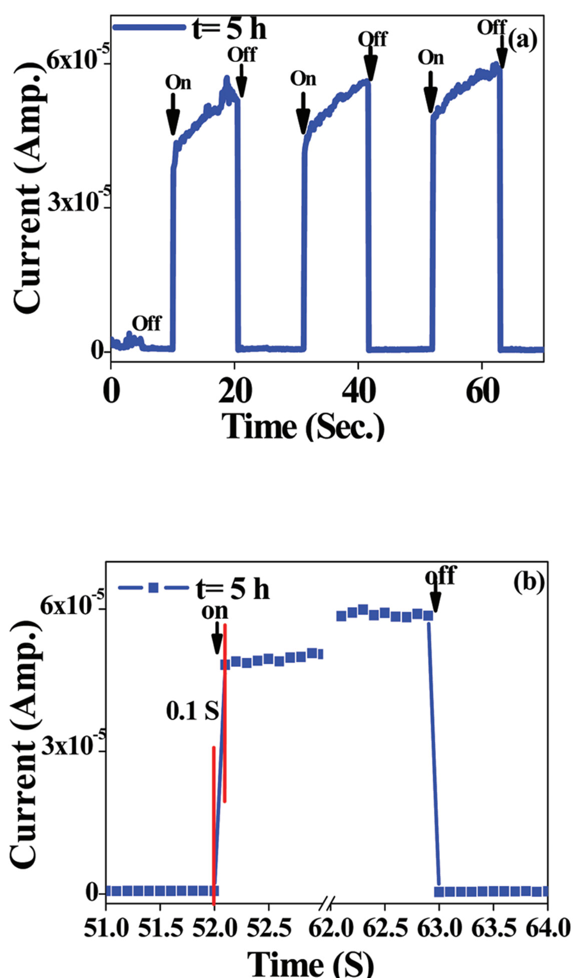

Figure 9. (a) Transient photoresponse by turning on-off visible light illumination of a representative heterojunction made by composite NRs. (b) Enlarged part of a transient cycle showing that the response and decay times are faster than 0.1 s.

■ CONCLUSIONS

In conclusion, we have demonstrated an entirely metal-free doping methodology involving the sulphidation technique to enhance the conductivity of ZnO NRs arrays. Without much sacrificing of the transparency of the NRs arrays, the current conduction by the layer is enhanced by as high as nearly 4 orders of magnitude. Therefore, we claim that the simple sulphidation process can lead to highly conducting ZnO NRs arrays without using a metal doping process which can be applied in cost-effective transparent electrodes in display devices as well as in photodiodes. This sulphidation process may be applied to increase the conductivity of similar metal oxide NRs without affecting the transparency of the NRs layer.

■ AUTHOR INFORMATION

Corresponding Author

*E-mail: sspdb@iacs.res.in. Fax : (91)-(33) 24732805.

Notes

The authors declare no competing financial interest.

■ ACKNOWLEDGMENTS

The authors acknowledge the HRTEM, XPS facilities provided by DST through the Unit of Nanoscience at IACS, India. One of the authors, S. Panigrahi, is thankful to CSIR, New Delhi, for awarding the senior research fellowship.

■ REFERENCES

(1) Law, M.; Greene, L. E.; Johnson, J. C.; Saykally, R.; Yang, P. D. *Nat. Mater.* **2005**, *4*, 455−459.
(2) Brown, P. R.; Lunt, R. R.; Zhao, N.; Osedach, T. P.; Wanger, D. D.; Chang, L. Y.; Bawendi, M. G.; Bulovic, V. *Nano Lett.* **2011**, *11*, 2955−2961.
(3) Qin, Y.; Wang, X. D.; Wang, Z. L. *Nature* **2008**, *451*, 809−813.
(4) Rout, C. S.; Kulkarni, G. U.; Rao, C. N. R. *J. Nanosci. Nanotechnol.* **2009**, *9*, 5652−5658.
(5) Liao, L.; Fan, H. J.; Yan, B.; Zhang, Z.; Chen, L. L.; Li, B. S.; Xing, G. Z.; Shen, Z. X.; Wu, T.; Sun, X. W.; Wang, J.; Yu, T. *ACS Nano* **2009**, *3*, 700−706.
(6) He, J. H.; Ho, C. H.; Chen, C. Y. *Nanotechnology* **2009**, *20*, 065503−065508.
(7) Hsu, Y. F.; Xi, Y. Y.; Yip, C. T.; Djurisic, A. B.; Chan, W. K. *J. Appl. Phys.* **2008**, *103*, 083114−083117.
(8) Qiu, J.; Guo, M.; Wang, X. *ACS Appl. Mater. Interfaces* **2011**, *3*, 2358−2367.
(9) Lupan, O.; Pauporte, T.; Viana, B.; Tiginyanu, I. M.; Ursaki, V. V.; Cortes, R. *ACS Appl. Mater. Interfaces* **2010**, *2*, 2083−2090.
(10) Lai, E.; Kim, W.; Yang, P. D. *Nano Res.* **2008**, *1*, 123−128.
(11) Jin, Y.; Wang, J.; Sun, B.; Blakesley, J. C.; Greenham, N. C. *Nano Lett.* **2008**, *8*, 1649−1653.
(12) Liu, J. S.; Shan, C. X.; Li, B. H.; Zhang, Z. Z.; Yang, C. L.; Shen, D. Z.; Fan, X. W. *Appl. Phys. Lett.* **2010**, *97*, 251102−251104.
(13) Sun, F.; Shan, C. X.; Li, B. H.; Zhang, Z. Z.; Shen, D. Z.; Zhang, Z. Y.; Fan, D. *Opt. Lett.* **2011**, *36*, 499−501.
(14) Rout, C. S.; Rao, C. N. R. *Nanotechnology* **2008**, *19*, 285203−285209.
(15) Fang, X.; Li, J.; Zhao, D.; Shen, D.; Li, B.; Wang, X. *J. Phys. Chem. C* **2009**, *113*, 21208−21212.
(16) Lupan, O.; Chai, G.; Chow, L.; Emelchenko, G. A.; Heinrich, H.; Ursaki, V. V.; Gruzintsev, A. N.; Tiginyanu, I. M.; Redkin, A. N. *Phys. Status Solidi A: Appl. Mater. Sci.* **2010**, *207*, 1735−1740.
(17) Mridha, S.; Basak, D. *J. Phys. D: Appl. Phys.* **2007**, *40*, 6902−6907.
(18) Xu, C. X.; Sun, X. W.; Chen, B. J. *Appl. Phys. Lett.* **2004**, *84*, 1540−1542.
(19) He, H.; Lao, C. S.; Chen, L. J.; Davidovic, D.; Wang, Z. L. *J. Am. Chem. Soc.* **2005**, *127*, 16376−16377.
(20) Hsu, C.-H.; Chen, D.-H. *Nanotechnology* **2010**, *21*, 285603−285610.
(21) Bera, A.; Ghosh, T.; Basak, D. *ACS Appl. Mater. Interfaces* **2010**, *2*, 2898−2903.
(22) Tang, Q.; Li, Y.; Zhou, Z.; Chen, Y.; Chen, Z. *ACS Appl. Mater. Interfaces* **2010**, *2*, 2442−2447.
(23) Cheng, C. W.; Sie, E. J.; Liu, B.; Huan, C. H. A.; Sum, T. C.; Sun, H. D.; Fan, H. J. *Appl. Phys. Lett.* **2010**, *96*, 071107−071109.
(24) Lin, J. M.; Lin, H. Y.; Cheng, C. L.; Chen, Y. F. *Nanotechnology* **2006**, *17*, 4391−4394.
(25) Panigrahi, S.; Basak, D. *Nanoscale* **2011**, *3*, 2336−2341.
(26) Bera, A.; Basak, D. *ACS Appl. Mater. Interfaces* **2010**, *2*, 408−412.
(27) Leschkies, K. S.; Divakar, R.; Basu, J.; Enache-Pommer, E.; Boercker, J. E.; Carter, C. B.; Kortshagen, U. R.; Norris, D. J.; Aydil, E. S. *Nano Lett.* **2007**, *7*, 1793−1798.
(28) Dutta, S.; Chattopadhyay, S.; Sarkar, A.; Chakrabarti, M.; Sanyal, D.; Jana, D. *Prog. Mater. Sci.* **2009**, *54*, 89−136.
(29) Zhou, Z.; Kato, K.; Komaki, T.; Yoshino, M.; Yukawa, H.; Morinaga, M.; Morita, K. *J. Electroceramics* **2003**, *11*, 73−79.
(30) Shen, G. Z.; Cho, J. H.; Jung, S. I.; Lee, C. J. *Chem. Phys. Lett.* **2005**, *401*, 529−533.
(31) Yousefi, R.; Kamaluddin, B. *Solid State Sci.* **2010**, *12*, 252−256.
(32) Hussain, S. G.; Liu, D. M.; Huang, X. T.; Sulieman, K. M.; Liu, J. P.; Liu, H. R.; Rasool, R. U. *J. Phys. D: Appl. Phys.* **2007**, *40*, 7662−7668.

(33) Shen, G. Z.; Cho, J. H.; Yoo, J. K.; Yi, G. C.; Lee, C. J. *J. Phys. Chem. B* **2005**, *109*, 5491−5496.
(34) Yousefi, R.; Kamaluddin, B. *Appl. Surf. Sci.* **2009**, *255*, 9376−9380.
(35) Bae, S. Y.; Seo, H. W.; Park, J. H. *J. Phys. Chem. B* **2004**, *108*, 5206−5210.
(36) Geng, B. Y.; Wang, G. Z.; Jiang, Z.; Xie, T.; Sun, S. H.; Meng, G. W.; Zhang, L. D. *Appl. Phys. Lett.* **2003**, *82*, 4791−4793.
(37) Sun, Y. P.; He, T.; Guo, H. Y.; Zhang, T.; Wang, W. T.; Dai, Z. H. *Appl. Surf. Sci.* **2010**, *257*, 1125−1128.
(38) Oba, F.; Togo, A.; Tanaka, I.; Paier, J.; Kresse, G. *Phys. Rev. B* **2008**, *77*, 245202−245207.
(39) Bera, A.; Basak, D. *Appl. Phys. Lett.* **2008**, *93*, 053102−053104.
(40) Pan, H. L.; Yang, T.; Yao, B.; Deng, R.; Sui, R. Y.; Gao, L. L.; Shen, D. Z. *Appl. Surf. Sci.* **2010**, *256*, 4621−4625.
(41) Chen, Y.-C.; Wang, C.-H.; Lin, H.-Y.; Li, B.-H.; Chen, W.-T.; Liu, C.-P. *Nanotechnology* **2010**, *21*, 455604−455611.
(42) Xu, J. F.; Ji, W.; Lin, J. Y.; Tang, S. H.; Du, Y. W. *Appl. Phys. A: Mater. Sci. Process.* **1998**, *66*, 639−641.
(43) Lu, S. W.; Schmidt, H. K. *Mater. Res. Bull.* **2008**, *43*, 583−589.
(44) Sann, J.; Stehr, J.; Hofstaetter, A.; Hofmann, D. M.; Neumann, A.; Lerch, M.; Haboeck, U.; Hoffmann, A.; Thomsen, C. *Phys. Rev. B* **2007**, *76*, 195203−195208.
(45) Zeng, H.; Duan, G.; Li, Y.; Yang, S.; Xu, X.; Cai, W. *Adv. Funct. Mater.* **2010**, *20*, 561−572.
(46) Vlasenko, L. S.; Watkins, G. D. *Phys. Rev. B* **2005**, *72*, 035203−035214.
(47) Gruzintsev, A.; Volkov, V.; Barthou, C.; Benalloul, R.; Frigerio, J. M. *Thin Solid Films* **2004**, *459*, 262−266.
(48) Shan, F. K.; Liu, G. X.; Lee, W. J.; Lee, G. H.; Kim, I. S.; Shin, B. C. *Appl. Phys. Lett.* **2005**, *86*, 221910−221912.
(49) Ong, H. C.; Du, G. T. *J. Cryst. Growth* **2004**, *265*, 471−475.
(50) Ilican, S.; Caglar, Y.; Caglar, M.; Yakuphanoglu, F.; Cui, J. *Physica E* **2008**, *41*, 96−100.
(51) Lin, J. M.; Zhang, Y. Z.; Ye, Z. Z.; Gu, X. Q.; Pan, X. H.; Yang, Y. F.; Lu, J. G.; He, H. P.; Zhao, B. H. *Appl. Surf. Sci.* **2009**, *255*, 6460−6463.
(52) Luo, L.; Zhang, Y. F.; Mao, S. S.; Lin, L. W. *Sens. Actuators, A: Phys.* **2006**, *127*, 201−206.
(53) Kar, J. P.; Kumar, M.; Choi, J. H.; Das, S. N.; Choi, S. Y.; Myoung, J. M. *Solid State Commun.* **2009**, *149*, 1337−1341.
(54) Fang, X.; Bando, Y.; Liao, M.; Gautam, U. K.; Zhi, C.; Dierre, B.; Liu, B.; Zhai, T.; Sekiguchi, T.; Koide, Y.; Golberg, D. *Adv. Mater.* **2009**, *21*, 2034−2039.
(55) Zhou, J.; Gu, Y.; Hu, Y.; Mai, W.; Yeh, P.-H.; Bao, G.; Sood, A. K.; Polla, D. L.; Wang, Z. L. *Appl. Phys. Lett.* **2009**, *94*, 191103−191105.
(56) Zhai, T.; Fang, X.; Liao, M.; Xu, X.; Li, L.; Liu, B.; Koide, Y.; Ma, Y.; Yao, J.; Bando, Y.; Golberg, D. *ACS Nano* **2010**, *4*, 1596−1602.
(57) Gao, T.; Li, Q. H.; Wang, T. H. *Appl. Phys. Lett.* **2005**, *86*, 173105−173107.
(58) Ohno, T.; Akiyoshi, M.; Umebayashi, T.; Asai, K.; Mitsui, T.; Matsumura, M. *Appl. Catal., A: Gen.* **2004**, *265*, 115−121.